International Journal of Mass Spectrometry 303 (2011) 212–219

Contents lists available at ScienceDirect

International Journal of Mass Spectrometry

journal homepage: www.elsevier.com/locate/ijms

Comparison of quadrupole mass filters with hyperbolic and cylindrical rods working in the third stability zone

Gianangelo Bracco[a,b,*]

[a] CNR-IMEM and Physics Department, University of Genoa, via Dodecaneso 33, I-16146 Genoa, Italy
[b] MIMT and Department of Physics and Technology, University of Bergen, Allegaten 55, 5007 Bergen, Norway

ARTICLE INFO

Article history:
Received 30 November 2010
Received in revised form 4 February 2011
Accepted 4 February 2011
Available online 21 February 2011

Keywords:
Quadrupole mass filter
Finite element method
Ion trajectory simulation
Mathieu stability diagram
Third stability zone

ABSTRACT

The working point of a quadrupole mass filter is generally set in the first zone of stability. For applications that require higher resolutions other stability zones can provide a suitable alternative and in this article it is investigated the third zone in particular for applications in the low mass range. Ion trajectory simulations for $^4He^+$ have been carried out for cylindrical as well as hyperbolic rods and the results have been compared. For cylindrical rods the best mass resolution has been obtained with a ratio between rod radius and field radius of 1.120. For this value further simulations have been performed to determine the dependence of transmission on the injection regions and injection angle in the quadrupole field. The analysis of the transmission regarding low and high mass tails has shown that it is possible to get rid of the low mass tails for cylindrical rods by limiting the injection region, instead the high mass tails, which affect the transmission for both cylindrical and hyperbolic rods, can be reduced by increasing the frequency of the radio frequency applied to the rods. Therefore, although the mass resolution at 50% of the peak height for hyperbolic rods is always greater than for cylindrical ones, with a suitable (reduced) ion injection region, the maximum transmission and the baseline resolution of a filter equipped with cylindrical rods can be made to approach that of a hyperbolic rod filter.

1. Introduction

Quadrupole mass filters (QMF) developed in the 1950s by Paul et al. [1–3] are largely used in many instruments for mass separation. Ideal mass filters are based on four rods with hyperbolic section to generate the appropriate electric field but in commercial instruments cylindrical rods are preferred due to the simplicity of construction although the generated field is perturbed with respect to the ideal case. A constant (dc) U and radio frequency (RF) V potentials are applied to the rods and ions injected in the quadrupole field oscillated in the plane (x, y) perpendicular to the QMF axis (z axis) with a trajectory described by the Mathieu equation [4]: ions with the selected mass oscillate with an amplitude which is limited (stable trajectory) while ions with other masses have trajectories with amplitude that increases with time and, if the time spent in the field is enough, they finally hit the rods and are rejected. It is useful to introduce the Mathieu parameters $a = 4eU/(m\omega^2 r_0^2)$, $q = 2eV/(m\omega^2 r_0^2)$, where m is the ion mass of charge e, $\omega = 2\pi f$ the angular frequency of the RF component and r_0 is the radius of the free region between rods, to parameterize the equation and discuss the stability conditions. In the (a, q) plane it is possible to separate regions where the ions have stable trajectories both along x and y as shown in Fig. 1. Commercial instruments generally operate in stability zone 1 (close to the vertex of the quasi-triangular region with $a = 0.237$, $q = 0.706$) [5] but for applications that require higher resolutions which are not feasible in the first zone, other stability zones can provide a suitable alternative [6–10]. Unfortunately increasing the (a, q) values for working in those zones, the (U, V) potentials applied to QMF rods are also increased and this could limit the higher mass value that can be transmitted. On the other hand, the low mass range up to 6 atomic mass units (amu) is an interesting range for applications such as helium leak detection and fusion research where the quantitative measurement of hydrogen isotopes is necessary along with the detection of small helium concentrations in a deuterium atmosphere [11–14]. In fact a $m/\Delta m$ resolution greater than 930 is necessary to separate HT^+ and D_2^+ [15], resolution not readily achievable with commercial instruments. Other interesting cases are for He beam scattering techniques [16–19] and in particular ^{3}He spin echo scattering [20] where $^3He^+$ has to be be detected in the presence of HD^+: this requires a resolution greater than 512 with a large transmission to increase the ^{3}He detected signal and a

* Correspondence address: CNR-IMEM and Physics Department, University of Genoa, via Dodecaneso 33, I-16146 Genoa, Italy. Tel.: +39 010 3536287; fax: +39 010 3622790.
E-mail address: bracco@fisica.unige.it

1387-3806/$ – see front matter © 2011 Elsevier B.V. All rights reserved.
doi:10.1016/j.ijms.2011.02.002

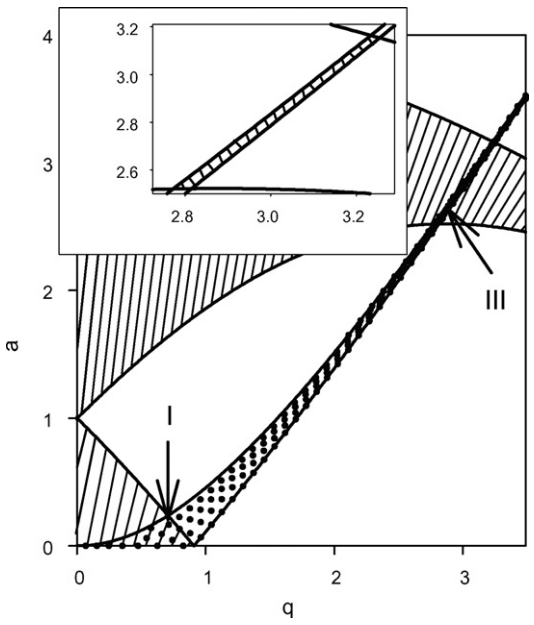

Fig. 1. Stability diagram for the solutions of the Mathieu equation with displayed first and third zones. Different shaded regions correspond to regions where ion trajectories are stable along x (shaded with solid lines) and along y (shaded with dotted lines). In the inset, the details of the third zone are shown.

very small contribution of the HD^+ signal on the ^3He mass, i.e., tail of the HD^+ transmission peak, which contribute to noise and limit the minimum detectable signal. Moreover the low mass range is advantageous since it can be scanned with a high number of mass steps across the mass peaks to achieve high resolution and the feasibility of this approach has been successfully demonstrated by Day [21] who used a modified QMF to separate $^4He^+$ and D_2^+.

In the present study, the performance of QMFs working in the third zone just below the upper vertex at $(q, a) = (3.23408, 3.16439)$ and equipped with hyperbolic and cylindrical rods has been investigated. In the case of cylindrical rods, the calculations have been initially performed for different values of r/r_0 to determine the optimal geometry which provides the best mass resolution. For this geometry, the analysis of the partial transmission [22,23] has been carried out to determine the injection regions with high transmission. In these simulations ions have been also injected with injection angles between zero (initial velocity parallel to QMF axis) and -15° (initial velocity converging towards the QMF axis). The last part of the article is dedicated to the study of low and high mass tails of the transmission peak and their different dependence on mass resolution, frequency and injection area. This analysis will show how it is possible to reduce or eliminate these tails. The present results add some new information to the findings of previous investigations [24,25] and can be useful for the construction of QMFs with cylindrical rods working in the third stability zone.

2. Field calculation and simulation methodology

Inside an infinite quadrupolar structure, the potential field ϕ is the solution of the Laplace equation $\nabla^2\phi = 0$. Assuming a cartesian orthogonal system with the origin on the quadrupole axis and with the x and y axes passing through the centers (focal points) of the circular (hyperbolic) sections of the cylindrical (hyperbolic) rods, the field can be expressed by a series of multipolar terms and imposing the symmetry requirement that the field must change sign when the azimuthal angle θ (angle between a radial direction and the x axis) is changed by $\pi/2$, the field with the appropriate symmetry is

$$\phi = (U + V\cos(2\pi ft))\sum_n B_n\left(\frac{r}{r_0}\right)^{2(2n+1)} cos(2(2n+1)\theta) \quad (1)$$

and by differentiating Eq. (1), the equations of motion for ion of mass m and charge e are expressed by

$$\frac{d^2x}{d\tau^2} = -(a + 2q\cos(2\tau))\sum_n (2n+1)B_n\left(\frac{x^2+y^2}{r_0^2}\right)^{(2n)} [x\cos(2(2n+1)\theta) + y\sin(2(2n+1)\theta)]$$

$$\frac{d^2y}{d\tau^2} = -(a + 2q\cos(2\tau))\sum_n (2n+1)B_n\left(\frac{x^2+y^2}{r_0^2}\right)^{(2n)} [y\cos(2(2n+1)\theta) - x\sin(2(2n+1)\theta)]$$

where a and q are the parameters defined above and $\tau = \omega t/2$, t is the time.

The ideal quadrupole field is given by the $n = 0$ term and the ion motion evolves independently on the two axes, instead the other higher order multipole terms

$$\sum_{n>0} B_n\left(\frac{r}{r_0}\right)^{2(2n+1)}\cos(2(2n+1)\theta) \quad (2)$$

act as a perturbation to the ideal case and couple the motions along the two axes modifying the stability condition.

The potential ϕ has been calculated by using a finite element method [23]. Part of the software was written as a FORTRAN code and part as MATLAB routines. The code related to the finite element method was written following Ref. [26] and the mesh is optimized following a procedure described in Ref. [27] which has been suitably modified for the present calculation.

In each calculation, the free space between opposite rods has radius r_0 and the rods are surrounded by a cylindrical case of radius $R = 3.54 \times r_0$ having a potential $\phi = 0$. After the calculation of ϕ, a fitting procedure is carried out to determine the coefficients B_n in Eq. (1) up to $n = 15$ which guarantee enough accuracy. The selected points are those which lie within the field radius r_0. Then the field gradient is analytically calculated for trajectory simulations. For hyperbolic rods it is assumed a single nonzero coefficient $B_0 = 1$ while for cylindrical rods the calculation of ϕ has been carried out for different values of r/r_0 in the range between 1.1 and 1.19.

The differential equations related to the motion of the ions are solved by using a fourth order Runge–Kutta algorithm. The time step has been decreased until no change has been observed on the results. The program generates ions in the first quadrant within a square S with sides of size d parallel to the positive x or y semiaxes and with a corner on the quadrupole (z) axis. For symmetry, the same behavior is expected for ions generated in similar squares located in the other three quadrants therefore the side of the complete injection region of the QMF is $2d$. As explained in Ref. [23], S is divided in N_C equal squared sub-units and, for each sub-unit, N_i ions are randomly generated with a uniform distribution in the sub-unit and in the time corresponding to a period of the RF component. In this way it is possible to correlate the transmitted percentage of ions with the starting sub-unit position as a function of the selected transmission mass (partial transmission) $T_i = 100 \times N_i^T/N_i$, where N_i^T is the number of transmitted ion separately counted for each sub-unit. For any mass step, the total number of particles $N = N_i \times N_C$ is injected in the field and the (total) transmission is $T = 100 \times \sum_{N_C}(N_i^T/N)$. For the present simulations $N_C = 400$ and N is between 8.6×10^6 and 17.2×10^6 ions.

Another type of simulation has been performed to investigate the dependence of the transmission on the injection angle χ (polar angle between the ion velocity and the z axis, negative values corresponds to ion trajectories converging towards the axis)and

azimuthal angle θ [23]. In fact, the ions are generally focused at the entrance of the QMF and their trajectories can form an angle χ with z. Due to the symmetry of the trajectories, positive or negative χ values give the same results as confirmed by the results of the simulations hence only negative values will be presented. For any azimuthal direction θ between 0° (x axis) and 90° (y axis) in steps of 15°, $N_A = 10^5$ ions are randomly generated with a uniform distribution in the time corresponding to a period of the RF component and are injected in the field with a constant χ. This is repeated for a set of 50 equally spaced points up to a distance $s/r_0 = 0.5$. The transmitted ions N_p are counted and the transmission for any point $T_P = 100 \times N_p/N_A$ is evaluated. For sake of clarity, the result will be presented for $\theta = 0°, 45°, 90°$ and for $\theta = 0°, -6°, -15°$.

All the simulations have been performed on ions with a kinetic energy of 5 eV and a mass corresponding to helium mass (4.0026 amu) which is at the center of the low mass region and for its importance in scattering experiments.

The length and field radius of the investigated QMF have been chosen as $L = 25$ cm and $r_0 = 3$ mm, respectively.

3. Results and discussion

In the first part of the investigation, the QMF has been simulated with a RF frequency of 4 MHz and the ions enter the quadrupole field with a velocity parallel to the z axis and $d = 0.5r_0$.

In a QMF, the frequency of the RF component is generally kept constant while the mass is scanned by varying the RF amplitude V in a suitable range and the dc amplitude U is a constant fraction of V, obtained by rectifying the RF component, and the mass resolution depends on the ratio $\gamma \propto U/V = 2q/a$. The coefficient of proportionality has been chosen such that the upper stability zone vertex of the third zone corresponds to $\gamma = 1$. The transmitted mass is expressed as

$$m = \frac{4e}{q \times \omega^2 r_0^2} V \tag{3}$$

and as, observed in Ref. [23], this mass scale works for a hyperbolic field ($B_0 = 1$) but for cylindrical rods B_0 is different from 1 and the mass scale

$$m' = B_0 \times m \tag{4}$$

seems more appropriate because it takes into account that the amplitude of the $n = 0$ (hyperbolic) term has a B_0-fold increase. The difference between these mass scales can be appreciated in Fig. 2a and b. The peak for the hyperbolic rods shows sharp leading and trailing edges, while the peaks associated to cylindrical rods display a tail on the low mass side. With the m scale the peaks for cylindrical rods are shifted with respect to the position of the hyperbolic case by increasing r/r_0. By using the m' scale, the peaks of cylindrical rods are distributed around the hyperbolic one: the peaks for r/r_0 greater than 1.120 (neglecting the low mass tails) start with a common leading edge almost at the leading edge of the hyperbolic case, instead the peaks for r/r_0 smaller than 1.120 end with a common trailing edge almost on the trailing edge of the hyperbolic case. The value 1.120 is therefore related to the minimum width Δm for cylindrical rods as shown in Fig. 3 where the mass resolution values, $m/\Delta m$, are depicted for Δm evaluated at 50% and 5% of the peak height.

On the other hand, the maximum transmission shows a minimum around 1.120, as displayed in Fig. 3 whose value is smaller than the transmission of hyperbolic rods. Therefore, the best mass resolution with cylindrical rods is obtained at the expenses of transmission. These results about transmission and mass resolution are consistent with the results of Ref. [25].

For the rest of the article, only the case with $r/r_0 = 1.120$, which displays the best $m/\Delta m$, will be considered.

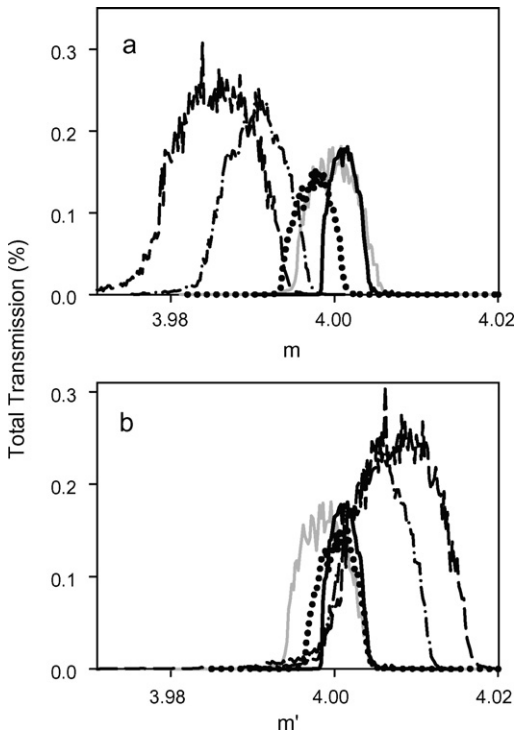

Fig. 2. Total transmission for quadrupole mass filters working in the third stability zone with $\gamma = 0.9995$ and equipped with hyperbolic (solid line) and cylindrical rods ($r/r_0 = 1.100$ (gray line), 1.118 (dotted line), 1.160 (dash dotted line), and 1.190 (dashed line)) for mass scales m (a) and m' (b), respectively. The size of the injection region is $d = 0.5r_0$.

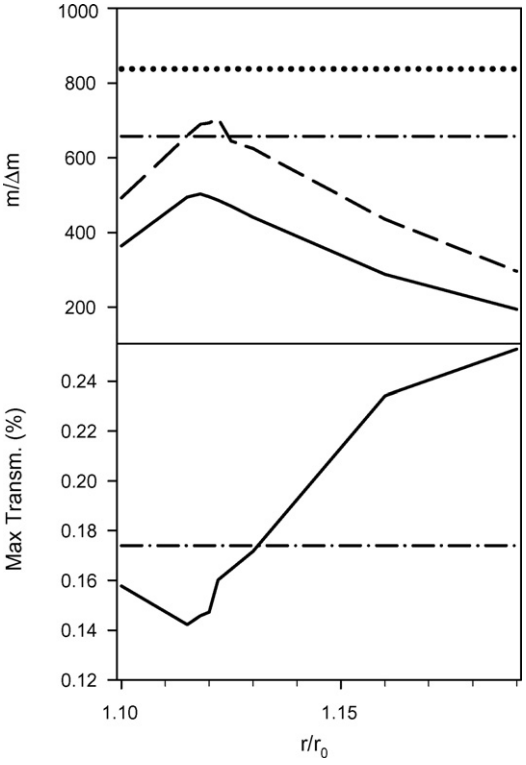

Fig. 3. Mass resolution $m/\Delta m$ evaluated at 50% (dashed line) and 5% (solid line) of the transmission peak height and maximum total transmission (solid line) for different r/r_0. The dotted and dash–dotted lines are related to the corresponding values for hyperbolic rods.

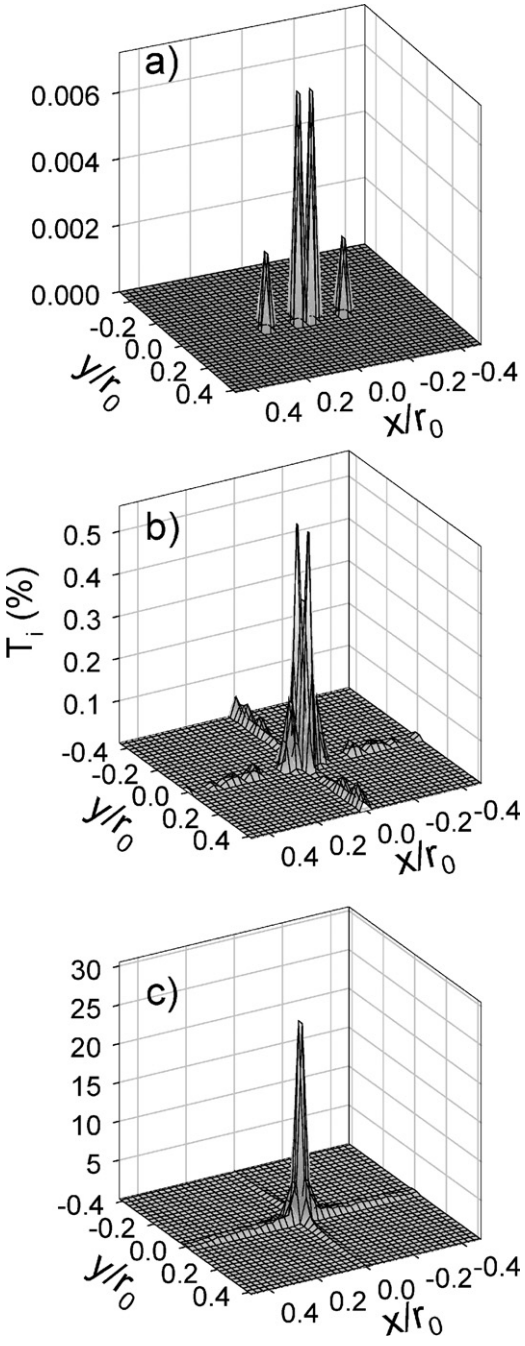

Fig. 4. Partial transmission T_i for cylindrical rods ($r/r_0 = 1.120$, $\gamma = 0.9995$) at $m' = 3.9878$ (a), 3.9970 (b), and 4.0026 (c).

The partial transmission T_i for cylindrical rods is shown in Fig. 4 at three different positions corresponding to the low mass tail (a), the leading edge (b), and the maximum (c) of the total transmission peak. The analysis of the starting sub-units shows that T_i in the low mass tail presents intensity only along the x axis with two very close peaks around the origin. At the leading edge of the peak, the intensity starts to be distributed also along the y axis and is mainly concentrated around the origin. At the maximum of the total transmission peak, the partial transmission is mainly concentrated in a single peak at the origin with small contributions along x and y. As a general observation, for all the masses, the intensity is only distributed along x and y axes (with generally more intensity along x) and is zero in the other regions. The results on the partial transmission

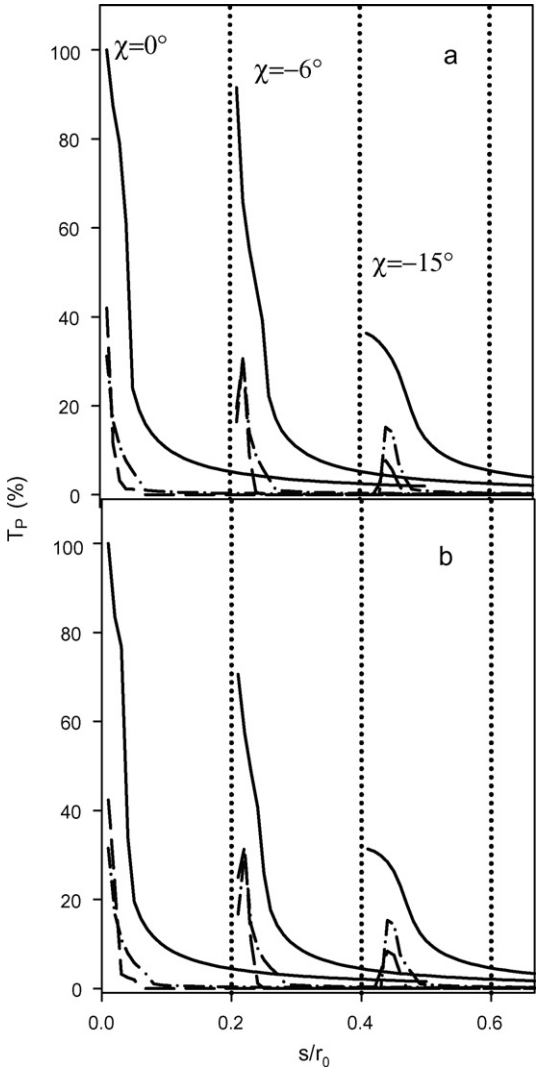

Fig. 5. Partial transmission T_P as a function of the distance from the origin s for different injection angle χ and different azimuthal angles θ: 0° (solid curves), 45° (dashed lines), and 90° (dot–dashed lines). The lines for $\chi = -6°$ are shifted by 0.2 s/r_0 while the lines for $\chi = -15°$ are shifted by 0.4 s/r_0. Simulations have been performed for $m' = 4.006$, $q = 3.23$, $a = 3.16$, and $\gamma = 0.9995$. Panel (a) displays the results for cylindrical rods ($r/r_0 = 1.120$) while panel (b) shows the results for hyperbolic rods.

will be analyzed with more details in the last part of the article.

The results of the simulations for injection with nonzero χ are shown in Fig. 5. For all the injection angles, the maximum transmission is always along $\theta = 0°$ (x axis) and it decreases with increasing χ. For $\chi = 0°$ the maximum occurs around the origin and this is true also for the other values along $\theta = 0°$. Instead, for $|\chi| > 0°$ and $\theta > 0°$, the maximum is shifted at $s/r_0 > 0$. For instance, for $\chi = -15°$, $\theta = 90°$, the maximum is located at about $s/r_0 = 0.04$. In any case, the transmission is concentrated in a region not exceeding $s = 0.1r_0$ and for greater distances the curves tend to zero with increasing s. Moreover, the curves for the QMF equipped with cylindrical rods are very similar to those ones related to hyperbolic rods.

The previous results show that limiting the entrance region of the filter to a size $d < 0.1r_0$, i.e., removing the regions with very low partial transmission, is beneficial for an increase of the transmission but it is not evident the impact of this reduction on the tails of the peaks. Moreover, the results for cylindrical rods are not so different from those related to hyperbolic rods and the main difference is the tail at low mass which is completely absent in the hyperbolic case.

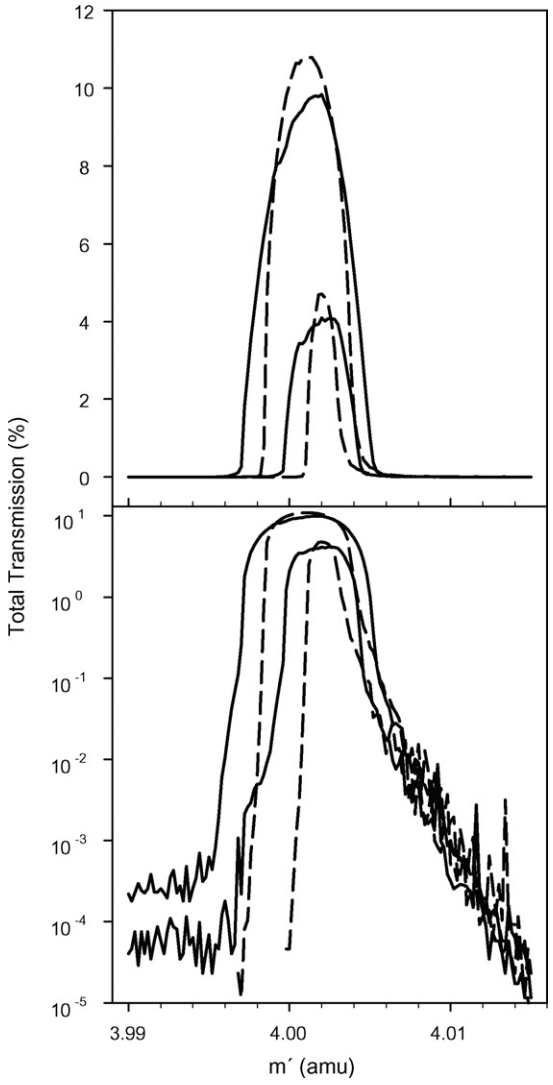

Fig. 6. Total transmission for cylindrical rods ($r/r_0 = 1.120$) (solid lines) and hyperbolic rods (dashed lines) at a frequency $f = 4$ MHz. The curves with higher transmission are calculated with $\gamma = 0.9995$ while the other with $\gamma = 0.9998$. A linear scale has been used in the upper panel while a semi-log scale is used in the lower panel.

The rest of the article is therefore dedicated to the analysis of the tails for a reduced injection region.

The results of simulation with a reduced injection region ($d = 0.05r_0$) and $\chi = 0^\circ$ are depicted in Fig. 6. As noted above, the maximum transmission is increased to about 10% for $\gamma = 0.9995$ and the comparison with the hyperbolic rods shows that the mass resolution is lower for the cylindrical case although the transmission is only ~1% lower. Increasing to $\gamma = 0.9998$, the mass resolution is increased and the transmission decreased to about 4%, still with a small difference between the two types of rods. Hence the resolution of cylindrical rods although is lower can follow that of the hyperbolic case with a small reduction of the transmission. In the lower panel of Fig. 6 the semi-log scale shows clearly the tails with fluctuations in the simulated signal due to the low ion counting and the random ion generation. As observed above, on the low mass side, only the cylindrical rods present a tail, between 4 and 5 order of magnitude smaller than the maximum transmission. The tail decreases very slowly going towards lower masses so its values appear almost constant. On the high mass side, both the cylindrical as well as the hyperbolic rods present quasi-exponential decreasing tails which coincide. Increasing γ, the tails are smaller but the ratio with the maximum transmission is almost the same for the

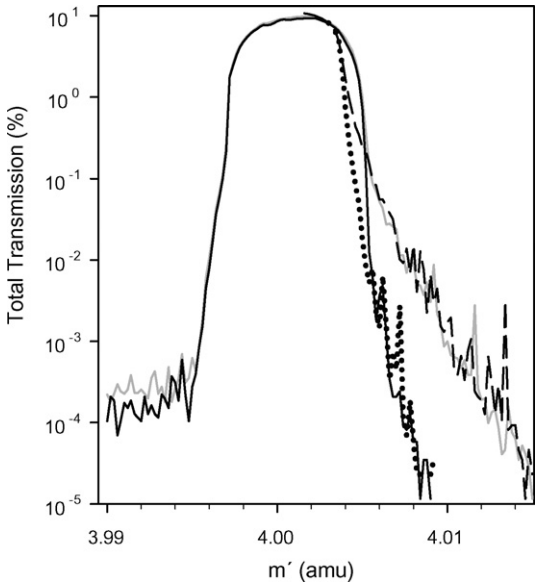

Fig. 7. Total transmission at $\gamma = 0.9995$ for cylindrical rods ($r/r_0 = 1.120$) (solid black line for $f = 6$ MHz, solid gray line for $f = 4$ MHz) and high mass tails for hyperbolic rods (dashed lines for $f = 4$ MHz, dotted line for $f = 6$ MHz).

low mass tail and, on the high mass side, the tails still coincide with a slope which is equal to that of the tails obtained for a smaller γ. Hence, the increase in mass resolution is not reducing the impact of the tails. The high mass tail for hyperbolic rods was also observed in Ref. [15] and the authors showed that an increase of f is necessary to reduce its values. In Fig. 7 the calculation at $f = 6$ MHz are displayed and compared with those at 4 MHz for cylindrical rods and, for sake of clarity, only the high mass tails of hyperbolic rods are shown. The shape of the peak is changed in a negligible way and the maximum transmission is reduced by less than 1%. On the other hand the decay of the quasi-exponential high mass tail is faster and with equal slope for cylindrical and hyperbolic rods. Instead, the low mass tail of the cylindrical case is not decreased appreciably.

Since neither an increase in mass resolution nor the frequency can reduce or avoid the presence of this low mass tail, the distribution of injected ion has been investigated with more detail. In Fig. 8, the partial transmission T_i is shown for $m' = 3.9922$ and 3.9962. At $m' = 3.9922$, the transmission is concentrated along x but with a gap of about $\pm 0.02x/r_0$ where the transmission in zero. A similar behavior has been observed in the region $m' < 3.9960$, on the left of the leading edge of the peaks shown in Fig. 6. For $m' = 3.9962$ some transmission starts to be present also along y but still around the origin the transmission is zero. This suggests that a further reduction of the injection could avoid the low mass tail for cylindrical rods. In Fig. 9 the peaks obtained for $d/r_0 = 0.05$, 0.025, 0.02, and 0.0125 are compared. The four limited injection regions determine an increase of the maximum transmission from about 10% to 27%, 36% and finally to 58%. The low mass tail extension is reduced: in fact the tail starts at $m' = 3.9910$, 3.9944, and 3.9970 for $d/r_0 = 0.025$, 0.02, and 0.0125, respectively and for smaller masses the transmission is zero. Reducing the injection region, the leading edge of the peak is steeper and the shoulder, which is visible up to $d/r_0 = 0.02$, completely disappears for 0.0125. The quasi-exponential high mass tail increases proportionally to the increase of the maximum transmission but the slope is not modified.

The transmission peak for cylindrical rods is without any low mass tails for $d/r_0 < 0.02$ and the high mass tail slope is not modified therefore it behaves similarly to the peak related to hyperbolic rods. In Fig. 10, for a reduced injection $d/r_0 = 0.0125$, the comparison between QMF equipped with cylindrical and hyperbolic

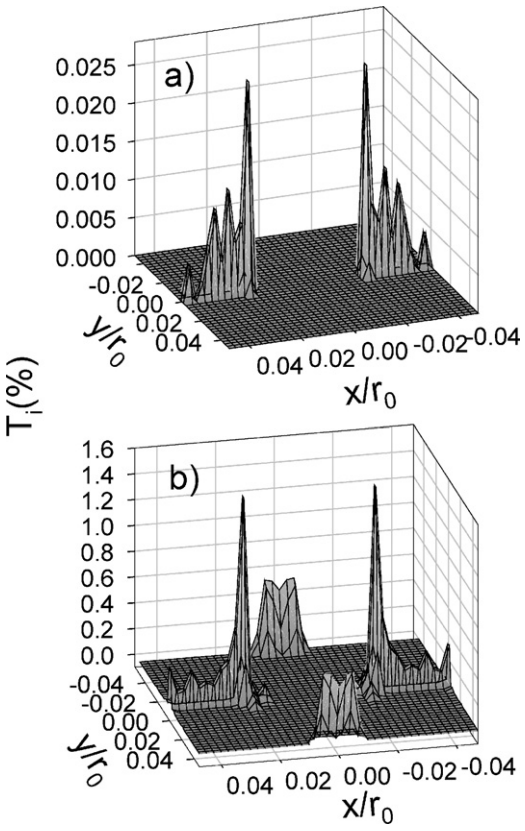

Fig. 8. Partial transmission T_i for cylindrical rods ($r/r_0 = 1.120$, $\gamma = 0.9995$, $f = 4$ MHz) at $m' = 3.9922$ (a) and $m' = 3.9962$ (b).

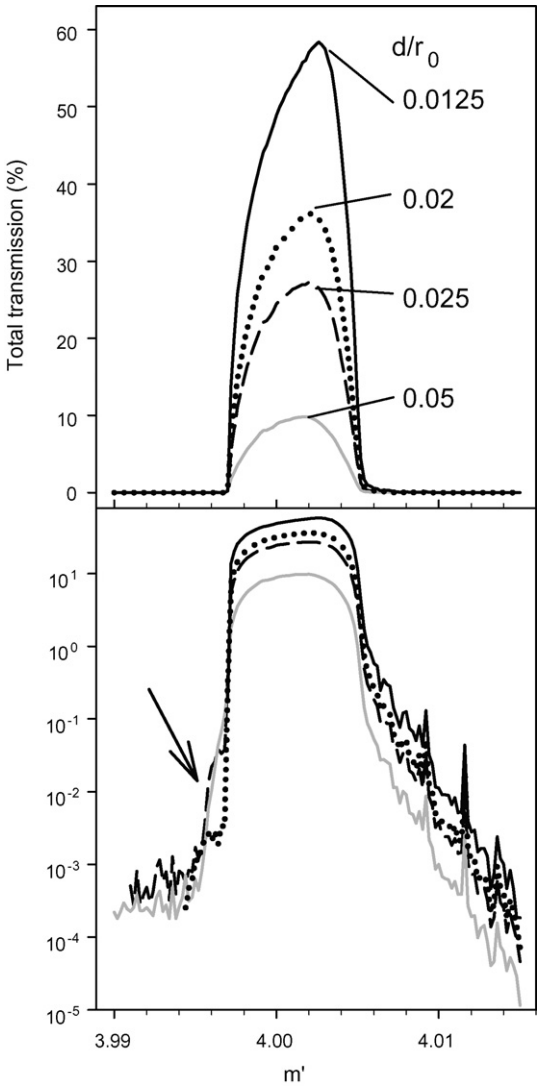

Fig. 9. Total transmission for cylindrical rods ($r/r_0 = 1.120$, $\gamma = 0.9995$, $f = 4$ MHz) for different injection regions: $d = 0.05r_0$ (a, solid gray line), $0.025r_0$ (b, dashed line), $0.02r_0$ (c, dotted line), and $0.0125r_0$ (d, solid black line). A linear scale has been used in the upper panel while a semi-log scale is used in the lower panel. The arrow indicates the region where the shoulders are present on the leading edge of the peaks.

rods is shown. The maximum transmission is the same and the mass resolution at 50% of the peak height is $m/\Delta m = 600$ and 800 for cylindrical and hyperbolic rods, respectively. The transmission starts to be different from zero at the same mass value and the slope of the high mass tail is the same.

The reduction of the QMF injection area causes a decrease of the measured ion current. It is useful to estimate the sensitivity of a QMF with cylindrical rods working in this condition and compare the estimated value with the sensitivity 10^{-7} A/mbar measured by Day [21] for a QMF with rod radius $r_D = 8$ mm working in the third zone of stability. The ion current can be calculated with a model of the QMF formed of three parts: the ionization source, the QMF with total transmission $T_t = T/100$ and the ion detector with detection efficiency E_D. In this model, each electron can generate a single ion and ion focusing is neglected. The ionization volume V can be assumed of cylindrical shape with a diameter which matches the QMF entrance aperture of size $2d$ and 1 cm length. The generated ions are injected in the QMF field with a probability p_i and are extracted with a probability p_e therefore the ion current can be calculated through the following relationship

$$I_{ion} = (\sigma_{ion} I_e N) p_i T_t p_e E_D \quad (5)$$

where σ_{ion} is the ionization cross section by electron impact for the considered atoms/molecules whose number at room temperature $N = 2.43 \times 10^{20} PV$ depends on their partial pressure P and the ionization volume V, I_e is the electron intensity. The He ionization cross section by electron impact at 110 eV is $\sigma_{He} = 3.7 \times 10^{-17}$ cm^2 [28] and a typical electron intensity is 1.2×10^{16} electrons/cm^2 s, i.e., a current density of 2 mA/cm^2. In measurements performed on the same QMF [29], the ion intensity in the third zone was between 2 and 5 times smaller than in the first zone and including a 50% for the injection probability in the first zone, a value $p_i = 0.1$ is assumed for the third zone. At the QMF exit, ions are accelerated towards the detector to energies above 1 keV and this accelerating potential allows an efficient ion extraction from the QMF field with $p_e \simeq 1$. Moreover for ions impinging on a channeltron with more than 1 keV, the ion detection efficiency is greater than 0.8 and this value has been assigned to E_D.

The estimated sensitivity for 8 mm rods and $2d = 0.04r_0 \simeq 0.29$ mm (corresponding to $T_t = 0.36$), is $I_{ion}/P = 3.3 \times 10^{-8}$ A/mbar, instead for $2d = 0.025r_0 \simeq 0.18$ mm ($T_t = 0.58$) the sensitivity is 2.1×10^{-8} A/mbar. These results show that the estimated sensitivity is at most 5 times smaller than the value measured by Day. On the other hand, this is an underestimation since at 110 eV each electron can ionize more than a single He atom [30] and ions generated in a larger volume could be focused on the entrance aperture, although the diameter of this volume has to be optimized to avoid too large injection angles (the decrease of transmission with injection angle is shown in Fig. 5). Moreover, the ion current could be also increased confining the electrons along the axis of the ion source by means of a magnetic field [31–34].

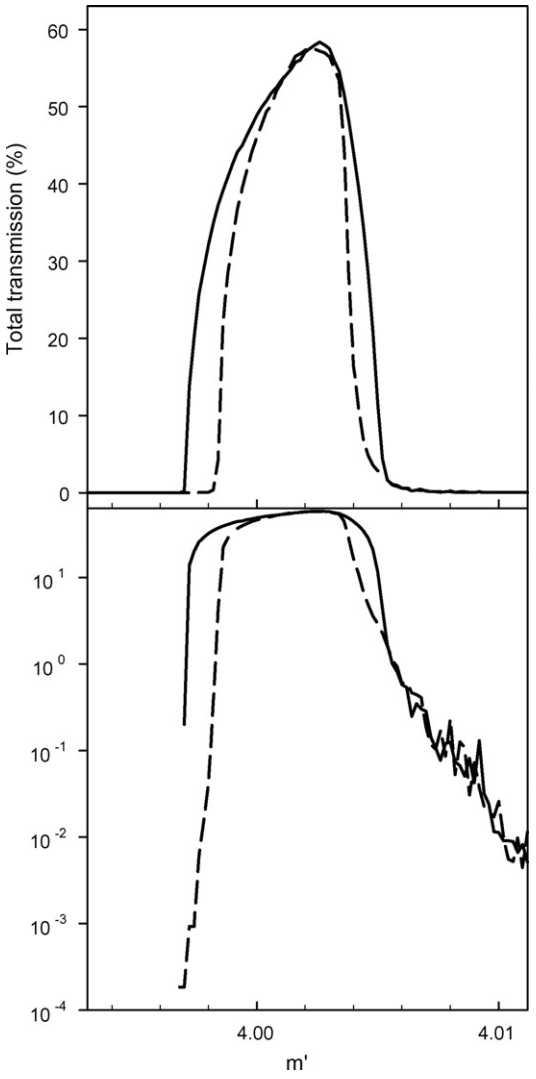

Fig. 10. Total transmission at $\gamma = 0.9995$, $f = 4$ MHz and $d/r_0 = 0.0125$ for cylindrical rods ($r/r_0 = 1.120$) (solid line) and hyperbolic rods (dashed lines). A linear scale has been used in the upper panel while a semi-log scale is used in the lower panel.

4. Conclusions

Trajectory simulations for $^4He^+$ ions have been performed for cylindrical as well as hyperbolic rods and the results have been compared. For cylindrical rods the best mass resolution has been obtained with $r/r_0 = 1.120$. For this value further simulations have been performed to determine the dependence of transmission on the injection angle in the quadrupole field and the injection regions where the partial transmission is higher. Analysis of the transmission has shown that the low mass tail can be reduced by limiting injection to the region $2d \leq 0.04r_0$. The high mass tail, which has a quasi-exponential decay, can be reduced for both cylindrical and hyperbolic rods by increasing the RF frequency. Therefore, although the mass resolution at 50% of the peak height for hyperbolic rods is always greater than for cylindrical ones, with a suitable (reduced) ion injection region, the maximum transmission and the baseline resolution of a filter equipped with cylindrical rods can be made to approach that of a hyperbolic rod filter.

The above analysis has been carried out for the injection of ions in a perfect field but, of course, fringing fields are present at the ion injection and extraction regions and this causes a loss of transmitted ions. In the first stability zone and to avoid this problem, Brubaker proposed the so called delayed dc ramp technique [35]: the four rods are separated in 2 parts, auxiliary rods near the entrance (pre-filter) and rods (filter). Only the RF component is applied to auxiliary rods therefore, going from the QMF entrance to the filter, both the dc and RF fields increase from 0 ($a = 0$, $q = 0$) to U and V, respectively, but the RF field reaches the regime value in the pre-filter instead the dc component increases to U only in the filter. Therefore the dc ramp is delayed with respect to the RF one. In the (a, q) plane, the ions with the selected mass follow a scan line which starts at the origin, it is along the q axis in the pre-filter where q reaches its regime value, and, when the ions enter the filter, the a value finally reaches its regime value. Hence the scan line is always inside the first stability zone avoiding transmission losses. In the case of the third stability zone, any scan line from the origin to the third zone has to cross a region where the ion trajectories are unstable. A pre-filter was tried [36] with a scan line which was close to the stability region along y (Fig. 1) but the results showed that for mass resolution greater than 120 the pre-filter does not improve the transmission.

The effect of fringing fields was analyzed [37,38] and it was shown that an optimal distance exists between the ends of the rods and entrance/exit plates that define the QMF external size. In fact an important parameter is the number n_F of RF cycles that an ion spends in the fringing field (which is related to the axial ion velocity) and the optimal values is $n_F = 1.2$. A complete three dimensional simulation of ions in the fringing fields is a highly demanding task for CPU and memory and some attempts are in progress to tackle this problem and estimate transmission and mass resolution.

References

[1] W. Paul, H. Steinwedel, Z. Naturforsch. A8 (1953) 448.
[2] W. Paul, M. Raether, Z. Phys. 140 (1955) 162.
[3] W. Paul, H.P. Reinhard, U. von Zahn, Z. Phys. 152 (1958) 143.
[4] N. McLachan, Theory and Application of Mathieu Functions, Oxford University Press, London, 1951.
[5] P. Dawson, N. Whetten, Advances in Electronics and Electron Physics, vol. 27, Academic, New York, 1969, p. 60.
[6] P.H. Dawson, Y. Bingoi, Int. J. Mass Spectrom. Ion Proc. 56 (1984) 41.
[7] N.V. Konenkov, V. Kratenko, Int. J. Mas Spectrom. Ion Processes 108 (1991) 115.
[8] C. Luo, D. Jiang, C. Ding, N.V. Konenkov, Rapid Commun. Mass Spectrom. 23 (2009) 2793.
[9] V.V. Titov, J. Am. Soc. Mass Spectrom. 9 (1998) 50.
[10] W. Chen, B.A. Collings, D.J. Douglas, Anal. Chem. 72 (2000) 540.
[11] R.E. Ellefson, W.E. Moddeman, H.F. Dylia, J. Vac. Sci. Technol. 18 (1981) 1062.
[12] S. Hiroki, T. Abe, Y. Murakami, Rev. Sci. Instrum. 63 (1992) 83874.
[13] S. Hiroki, T. Abe, Y. Murakami, Rev. Sci. Instrum. 65 (1994) 1912.
[14] A. Frattolillo, A. De Ninno, Proceedings of the 22nd IEEE Symposium on Fusion Engineering, Albuquerque, NM, June, 2007.
[15] J. Sreekumar, T.J. Hogan, S. Taylor, P. Turner, C. Knott, J. Am. Soc. Mass. Spectrom. 21 (2010) 1364.
[16] G. Bracco, J. Acker, M.D. Ward, G. Scoles, Langmuir 18 (2002) 5551.
[17] G. Bracco, R. Tatarek, G. Vandoni, Phys. Rev. B 42 (1990) 1852.
[18] G. Bracco, L. Bruschi, R. Tatarek, A. Franchini, V. Bortolani, G. Santoro, Europhys. Lett. 34 (1996) 687.
[19] M. Koch, S. Rehbein, G. Schmahl, T. Reisinger, G. Bracco, W.E. Ernst, B. Holst, J. Microsc. Oxford 229 (2008) 1.
[20] A.P. Jardine, H. Hedgeland, G. Alexandrowicz, W. Allison, J. Ellis, Prog. Surf. Sci. 84 (2009) 323–379.
[21] C. Day, Vacuum 51 (1998) 21.
[22] A.C.C. Voo, R. Ng, J.J. Tunstall, S. Taylor, J. Vac. Sci. Technol. A 15 (4) (1997) 2276.
[23] G. Bracco, Int. J. Mass Spectrom. 278 (2008) 75.
[24] P. Turner, S. Taylor, J.R. Gibson, J. Vac. Sci. Technol. A 23 (3) (2005) 480.
[25] T.J. Hogan, S. Taylor, IEEE Trans. Instrum. Meas. 57 (2008) 498.
[26] J. Alberty, C. Carstensen, S.A. Funken, Numer. Algorithms 20 (1999) 117.
[27] P.-O. Persson, G. Strang, SIAM Review 46 (2) (2004) 329.
[28] M.B. Shah, D.S. Elliott, P. McCallion, H.B. Gilbody, J. Phys. B: At. Mol. Opt. Phys. 21 (1988) 2751.
[29] Z. Du, T.N. Olney, D.J. Douglas, J. Am. Soc. Mass Spectrom. 8 (1997) 1230.
[30] K. Kuhnke, K. Kern, R. David, G. Comsa, Rev. Sci. Instrum. 85 (1994) 3458.
[31] C.J. Parka, J.R. Ahn, Rev. Sci. Instrum. 77 (2006) 085107.
[32] A.R. Alderwick, A.P. Jardine, H. Hedgeland, D.A. MacLaren, W. Allison, J. Ellis, Rev. Sci. Instrum. 79 (2008) 123301.

[33] M. DeKieviet, D. Dubbers, M. Klein, U. Pieles, C. Schmidt, Rev. Sci. Instrum. 71 (2000) 2015.
[34] A.V. Kalinin, L.Yu. Rusin, J.P. Toennies, Instrum. Exp. Technol. 49 (2006) 709.
[35] W. Brubaker, Advances in Mass Spectroscopy, vol. 4, Elsevier, Amsterdam, 1968, p. 293.
[36] S. Hiroki, K. Sakata, N. Sugiyama, S. Muramoto, T. Abe, Y. Murakami, Vacuum 46 (1995) 681.
[37] N.V. Konenkov, J.T. Dowell, Int. J. Mass Spectrom. Ion Processes 164 (1997) 201.
[38] N.V. Konenkov, Int. J. Mass Spectrom. Ion Processes 123 (1993) 101.